

Liquid Phase Flash Sintering in Magnesia Silicate Glass-Containing Alumina

Corresponding author: Mattia Biesuz¹

mattia.biesuz@unitn.it

+39 0461 283940

Vincenzo M. Sglavo^{1,2}

vincenzo.sglavo@unitn.it

¹University of Trento, Department of Industrial Engineering

Via Sommarive 9, 38123 Trento, ITALY

²INSTM, Trento UdR, Firenze-Italy

Publisher version available at:

<https://www.sciencedirect.com/science/article/pii/S0955221916304721>

Abstract

Magnesia silicate glass-containing alumina was flash sintered using an E-Field in the 500-1500 V/cm range. The addition of glass allows to reduce the current needed for densification and improves the shrinkage obtained during field-assisted sintering process. This behaviour is related to the different sintering mechanisms involved in the two materials, i.e. solid state sintering for pure alumina and liquid phase sintering for glass-containing alumina.

The estimated activation energy for conduction at FS is compatible with ionic diffusion in silicate melt. Moreover, evidence of magnesium diffusion toward the cathode is recorded.

The estimated sample temperature is in almost all cases lower than 1355°C, which is the temperature at which the first liquid is formed in the ternary system MgO- SiO₂ -Al₂O₃. Finally, it is shown that the application of an E-Field accounts for efficient liquid phase sintering at temperatures at which it cannot be reproduced conventionally.

Keywords: flash sintering, liquid phase sintering, alumina, glass softening

1 Introduction

Field Assisted Sintering (FAS) techniques represent one of the more promising routes for reducing sintering time and temperature of ceramic materials. Several research studies have been carried out in the last five years specifically on Flash Sintering (FS), showing that the densification process can be completed in just a few seconds at temperatures much lower than those required for conventional procedures. FS has proved to be a very efficient and effective sintering technique in ceramics with different electrical properties: high temperature ionic [1-12] and protonic [13] conductors, semiconductors [14], composites [15-17], electronic conductors [18-20] and insulators [21,22]. Such unusual behaviour is also followed by an anomalous drop in material resistivity. Although a thermal runaway from Joule heating has been proven to occur along flash sintering [4,17,23], the mechanisms leading to densification and the electrical behaviour are still not completely clear.

Very recent research has shown that the softening temperature of glass can be drastically reduced by the application of an electric field [24,25]. Such anticipated electric field-induced softening has been observed in some alkali-silicate glasses under DC polarization [24]. In these materials a non-conventional conduction behaviour also was observed, showing a sharp and unexpected increase of electrical conductivity of the glass.

Nowadays, many traditional and advanced ceramics are consolidated using a liquid-phase sintering process whereby the presence of a relatively small amount of liquid at high temperature promotes additional densification mechanisms [26].

A recent work by Gonzales-Julian et al. [27] has shown that the application of a moderate electrical field enhances the densification process of lime-silicate glass-containing alumina at high temperature (1450°C).

The goal of the present work is to extend the application of flash sintering - used so far only on materials characterized by solid state sintering mechanisms - to a very common and technologically important ceramic system, namely magnesia-silica glass-containing alumina. The specific aim was to explore the combined effect of electric field-induced glass softening and flash sintering to decrease sintering temperature and time of α -Al₂O₃ containing 10 wt% magnesia-silicate glass.

2 Experimental Procedure

Nearly pure α -alumina (Almatis CT3000SG, d_{50} = 0.6 μ m) was used in the present work. The nominal composition is: Al₂O₃ 99.8wt% - MgO 0.04wt% - Na₂O 0.03wt% - Fe₂O₃ 0.015wt% - SiO₂ 0.015wt% - CaO 0.015wt%. The vitreous phase was produced by sol-gel method from TEOS (Sigma Aldrich) and magnesium nitrate hexahydrate (Sigma Aldrich) as silica and magnesia precursor, respectively. TEOS and magnesium nitrate were dissolved in 2-propanol; then, 10% NH₄OH water solution was added for TEOS hydrolysis. The resulting suspension was dried overnight at 100°C. The obtained powder was then added to alumina and ball milled in 2-propanol for 3 hours. The suspension was dried and calcined in a muffle furnace under static air using a heating rate of 10°C/min up to 750°C (soaking time = 30

min). The nominal composition of the powder was α -Al₂O₃ 90 wt%, SiO₂ 8 wt%, MgO 2 wt%. Pure alumina powder was used also, for comparison.

The powder was uniaxially pressed in dog-bone-like samples using 7 wt% water as binder. The gage cross-section of the specimens was around 3x3 mm². One small hole was produced on each flared region of the dog-bone sample for electrical connection. The green samples were placed into an alumina dilatometer (Linseis L75) and connected by two platinum wires to a DC power supply (Glassman EW series) and a multimeter (Keithley 2100). A drop of platinum paste (Sigma Aldrich) was added into the holes in order to improve electrical contact between the green body and the wires.

The samples were heated at a rate of 20°C/min. Once the temperature reached 300°C, the power supply was turned on and the system started to work in voltage control. Fields in the 500-1500 V/cm range were used for the treatments. When the set current limit was reached, the system was left to work for 2 min in current control; then, power supply and furnace were shut down. Nominal current density in the range of 0.6-2 mA/mm² was applied to the glass-containing alumina (GCA) samples; pure alumina (A) specimens were studied only at 2 mA/mm², for comparison.

The samples' microstructure was characterized via SEM (Jeol JSM-5500). The apparent density was determined by Archimede's method, using an analytical balance with sensitivity ± 0.0001 g (Gibertini). For this analysis only the gage of the dog-bone samples (where the current density can be easily calculated) was taken into account. EDS analysis was carried out using Jeol IT300 SEM equipped with XFlash 630M detector (Bruker Quantax).

3 Results and Discussion

3.1 Densification Behaviour

Both the glass-containing alumina and the pure alumina samples were flash sintered under fields exceeding 500 V/cm. Figure 1 shows the dilatometric plots for the two materials using 2 mA/mm² nominal current limit. One can clearly observe that the glass addition accounts for a drastic increase in sintering rate, and this leads to greater shrinkage upon sintering. This is probably due the formation of a ternary liquid phase that enhances the densification mechanisms. Therefore, the results show clearly that flash sintering is a very effective technique for improving also the densification of glass-containing ceramic systems. An exception is represented by the samples sintered under 1500 V/cm; in such cases the current limit in the GCA system is reached at a very low furnace temperature (650-750°C) but no significant densification and shrinkage are achieved. Although a definitive explanation can not be drawn, this could be accounted for by the very low furnace temperature, which results also in a lower sample temperature during the flash. Using the well-known power balance equation for flash sintering [2, 4, 22] and assuming an emissivity between 0.5 and 0.9, the estimated temperature of all samples treated under 1500 V/cm ranges between 933 and 1310°C; such values are far below the lowest *liquidus* temperature of the ternary system (1355°C), thus not allowing the formation of a liquid phase.

The dilatometric curves for the GCA samples show two shrinking events. The first one occurs at a lower temperature and produces a moderate shrinkage of the sample (~2%). This is quite likely associated to softening in the vitreous phase, which allows for the rearrangement of the solid alumina particles. The second event, which takes place more rapidly at a higher temperature and is responsible for most of the shrinkage, is related to flash sintering and occurs once the current limit is reached.

The porosity and density data collected from the sintered bodies are shown in Figure 2. One can observe that the current density is controlling the densification behaviour and using

only 2 mA/mm² the apparent porosity of the GCA system is reduced to less than 4%. Moreover, especially if low currents are applied, there is a quite strong correlation between the applied voltage and the physical properties of the sintered bodies. In particular, the material becomes denser by decreasing the voltage, as a result of the higher onset temperature for flash sintering. As a matter of fact, the samples treated under lower fields are already partially shrunk and thus densified when the current limit is reached.

No significant differences are observed among samples treated using different fields especially when higher currents are used. The samples treated using 1500 V/cm are always not densified and the behaviour is weakly related to the applied current. In fact, by increasing the nominal current density from 0.6 to 2 mA/mm², the differences in terms of bulk density and open porosity appears negligible.

Figure 3 compares bulk density and open porosity for GCA and A systems. As expected from the dilatometric tests results, densification is enhanced by the addition of glass to alumina powder. In particular, GCA samples feature much lower open porosity. The differences are less evident in terms of bulk density, although one should consider that the theoretical density of the two materials is not the same: assuming that, after sintering, the glassy phase load is still 10 wt%, if densities of 2.20 and 3.95 g/cm³ are considered for glass and alumina, respectively, then the theoretical density of GCA material is 3.66 g/cm³, lower than that of pure alumina (3.95 g/cm³). An exception is represented, once again, by the GCA samples sintered under 1500 V/cm: such specimens are not dense and feature a relevant amount of open pores.

Figure 4 shows the fracture surface of pure alumina and glass-containing alumina specimens. All SEM micrographs refer to the central part of the gage portion of the dog bone sample. If the same current density is used, the glass-containing material is denser

than pure alumina and characterized by more limited porosity, in good agreement with the density measurements. This means that with the glass addition it is possible to achieve the same densification using lower current density and power dissipation. This has a significant beneficial role because it allows to avoid some technological problems related to electrode melting, partial reduction of the material and sparking, which are often observed in the case of high current applications. In addition, the two materials show a very different microstructure. The fracture mechanism is intergranular and transgranular in A and GCA system, respectively, this being associated to different densification mechanisms: it should not come as a surprise that the micrographs resemble solid state sintering – produced structure for pure alumina, while for glass-containing alumina the activation of a glassy phase upon densification shall be considered. Such evidence confirms that a liquid is formed during the sintering process of GCA, which is responsible for the differences observed in the densification behaviour. Another likely event is that, even when the current density is reduced down to 0.6 mA/mm^2 in GCA (Fig. 4(c)), a liquid phase sintering is observed.

Additional features can be analysed from observing polished and HF-etched cross-sections from GCA samples. Etching was carried out using 10% HF water solution for 25 s. Figure 5 compares the polished surface before and after HF-etching: it is possible to observe that a large amount of porosity is opened by etching. This suggests that a large amount of glassy phase is present in the sintered sample; in other words, the glass is not completely crystallized during the sintering process. It should also be pointed out that pores that open upon etching are characterized by a very stretched and sharp shape (Fig. 5(c)). This clearly indicates that the glass was able to flow between the alumina grains during the sintering process. This confirms that in the glass-containing material a liquid phase flash sintering process took place.

3.2 Sintering Temperature and Electrical Behaviour before FS

The relationship between the onset temperature for FS and the applied voltage is shown in Figure 6. One can observe that in the A system the behaviour is regular with an “exponential-like” shape. This behaviour has been successfully observed in a previous work using the thermal runaway model [22]. Conversely, GCA material behaves in a quite irregular way: under a higher field (1500 V/cm), the sintering event is anticipated with respect to pure alumina by more than 200°C. However, by decreasing the voltage (750 - 1250 V/cm), glass containing samples are flash sintered at higher temperatures.

At low temperatures (generally less than 970-870°C), glass-containing alumina powder is more conductive than pure alumina powder and this results in higher specific power dissipation in the GCA system, as shown in Figure 7(a). In fact, since the system works in voltage control before FS, the specific power dissipation can be calculated as [4,32,33]:

$$P_{(T)} = E^2 / \rho_{(T)} \quad (1)$$

where $\rho_{(T)}$ is the material resistivity and E the electrical field.

Different activation energy for conduction was also estimated from the power dissipation plots, from the slope in the low temperature region characterized by a linear-like behaviour (right portion of the diagrams in Fig. 7). In particular, the activation energy was 0.7 ± 0.1 and 1.2 ± 0.2 eV for GCA and A samples, respectively. This suggests that at low temperature the glassy phase is more conductive than alumina and plays a central role in the charge transport mechanisms. One can see that the calculated activation energy is much lower than the literature data reported for Si^{4+} , O^{2-} and Mg^{2+} diffusion in silicate minerals and glasses, these ranging between 2.0 and 4.3 eV [28-31,35]. In addition, the band gap for electron promotion in fused silica is much higher (8.3 eV) [33]. The reasons for such

unexpected behaviour can be related to some characteristics of the glassy phase. One should consider that the glass was produced by sol-gel method and therefore the obtained material is quite different from conventional glass. Other authors have already pointed out that glasses obtained by sol-gel methods are characterized by lower activation energy for ionic species diffusion, their diffusivity being more than one order of magnitude higher than that of bulk vitreous materials [42].

At higher temperatures, usually in the 820-1000°C range, the power dissipation plot of the glass-containing samples presents a certain instability. First, the slope of the curve starts increasing (as it happens just before FS) but after a few minutes the concavity turns downward (Figure 7). In this temperature range, the GCA system becomes more resistive (Fig 7(a)) when compared to pure alumina. This results in a delayed FS event for the glass-containing samples.

For a better understanding of the observed phenomenon a DSC analysis (NETZSCH DSC404, Pt crucible) was carried out on the GCA powder (Figure 8) using the same heating rate of the FS process (20°C/min). The plot shows an exothermic effect starting around 860°C. This peak is probably at the base of the described instability of the power dissipation plot. By way of comparison, two X-ray diffraction analyses were performed on the glass powder before and after thermal treatment at 950°C (heating rate = 20°C/min). It was shown that a large amount of glass is still present after the treatment, although some magnesium silicate crystalline phase (Enstatite) was found. Therefore, the exothermic peak in Fig. 8 can be ascribed to a partial crystallization of the glassy phase. Very likely, the crystallization event increases the resistivity of the glass and it is what causes the irregular electrical behaviour observed in GCA samples. This accounts for the higher onset temperature for flash sintering

when the current limit is reached after crystallization; conversely, FS is anticipated when the field is high enough to produce the runaway below 860°C.

If a relatively low field (500 V/cm) is used, the current limit is reached more or less at the same temperature by the GCA and A samples alike (Figure 4). The reason for this behaviour is probably connected to the fact that the GCA specimens shrink more than alumina upon heating. Being the voltage constant, this leads to moderate field intensification, which can explain an anticipated FS event, even if it occurs above 860°C.

If a very high field is applied (1500 V/cm), the slope of the power dissipation plot for GCA specimens changes (Figure 7 (b)). In this case, the activation energy was estimated to be 1.6 eV, significantly higher than that measured under lower voltages (0.7 eV). This indicates the presence of a non-linear conduction behaviour and a “field-induced” activation of different charge transport mechanisms. The enhancement in conductivity has already been reported and studied using very high fields in several glassy oxide systems and it is related to the asymmetry induced by the field in the energy barrier for diffusion [33,34]. One can also observe that the current limit is reached before the previously discussed partial crystallization of the glass. This means that the material is flash sintered in the temperature range in which the glass is much more conductive than alumina. The fact that alumina is probably not completely involved in charge transport mechanisms is another reason that can be claimed for explaining the limited densification of such specimens.

Finally, Figure 6 shows that the field also influences the temperature at which the maximum shrinkage rate is reached during glass softening. This parameter is obviously related to the glass-softening temperature and it is possible to refer to it as an indicator of the amorphous phase behaviour. In particular, in the tests carried out at 750-1250 V/cm, this reference temperature is only anticipating the flash sintering by 80-110°C. Therefore, it behaves in a

way similar to that of the onset temperature for FS. The correlation between the temperature at which the maximum shrinkage rate is reached during glass softening and the applied field can be accounted for by the Joule heating phenomenon that always precedes the achievement of the current limit. Nevertheless, at 750 V/cm the reference temperature reaches a plateau and it changes by just a few degrees when the field decreases down to 0 V/cm. This means that the glassy phase behaviour before FS is independent from the applied field. It may suggest that the glass is not particularly involved in charge transport phenomena in the temperature range between the described crystallization and FS.

3.3 Electrical Behaviour during FS

Material resistivity was estimated during FS. In particular, the data collected in the second minute after the FS event were analysed in order to make sure that the system was stable enough and that the specimen temperature was relatively constant. The real resistivity of the system was calculated considering that in all specimens a certain amount of porosity was still present during the process. All values were estimated under the following hypothesis:

- i. Most of the densification occurs in the first minute after FS;
- ii. The porosity is homogeneously distributed;
- iii. The density of the material can be approximated to that previously measured.

Figure 9 shows resistivity as a function of the estimated sample temperature. As expected, a log-log relation can be observed. The resistivity ($\rho_{(T)}$) in ceramic oxide materials typically scales with temperature according to the following equation:

$$\ln(\rho_{(T_s)}) = \ln(\rho_0) + Q/RT_s \quad (2)$$

where ρ_0 is a pre-exponential constant, Q the activation energy for conduction, R the universal gas constant and T_s the sample temperature.

The sample temperature can be estimated assuming that all the heat is exchanged by radiation; therefore, the power balance can be written as [2, 4, 22]:

$$EJV = \sigma \varepsilon S (T_s^4 - T_F^4) \quad (3)$$

where E is the field, J the current density, V and S the sample volume and surface, respectively, σ the Stefan- Boltzmann universal constant, ε the material emissivity and T_F the furnace temperature.

The experimental data were fitted using different emissivity values in the 0.2-1 range. The best fit was obtained using an emissivity of 0.54 and an activation energy of 2.5 eV. It is possible to specify that the estimated emissivity is in the range of the data available in the literature (0.4-0.8) [43-45]. Conversely, the activation energy is much higher than that previously calculated from the power dissipation plots (0.7 eV). Even by changing the emissivity in a wide range (0.2-1), the activation energy is always higher than 1.1 eV, not comparable with the results obtained previously. In addition, one can observe that the estimated activation energy for conduction during FS in GCA (2.5 eV) is far higher than that calculated in previous studies for pure alumina (0.76 eV) [22].

Therefore, it is possible to state that:

- i. The conduction behaviour during FS is different from that observed before the current limit is reached.
- ii. The conduction mechanisms during FS in pure alumina and glass-containing alumina are undoubtedly different, and this suggests that the vitreous phase is mainly involved in the charge transport mechanisms.

The activation energy for Flash Sintering is compatible with ion diffusion phenomena in molten silicates: values in the 1.1-2.9 eV range have been previously reported for Si^{4+} , Mg^{2+} and O^{2-} diffusion [35-40]. One can observe that this value is far lower than the band gap for electron promotion in fused silica and alumina [32]. Therefore, the current is flowing in the vitreous phase during FS and, probably, the conduction is based on ionic diffusion.

In order to verify the presence of ionic conduction phenomena in the foregoing flash sintering experiments, the concentration profiles of Mg and Al were recorded by EDS close to the cathode and the anode of some FS specimens. Figure 10 shows the data collected on the sample treated with 2 mA/mm² and 750 V/cm. One can see that the relative concentration of Mg is much higher at the cathode and progressively decreases moving away from the electrode, reaching a plateau after about 700 μm . Conversely, a lower Mg concentration was measured around the anode. In this case, the Mg signal increases with the distance from the electrode and it hits a constant value after about 250 μm . At larger distances the Mg concentration does not change significantly.

Mg diffusion was also analysed by recording some EDS concentration maps near the cathode. As shown in Figure 11, a strong magnesium signal was recorded very close to the electrode: a homogeneous and thin Mg-rich layer around the hole where the platinum wire was inserted is visible. By increasing the field ($E \geq 1000$ V/cm), the magnesium-enriched zone becomes wider. Such area is also characterized by a different microstructure (it is denser) and can probably be associated to some kind of discharge due to the high field and power dissipation.

No significant Si^{4+} diffusion was observed by EDS. As shown in Figure 11, silicon concentration is always constant. This result is not surprising: since silicon is a glass network former, its mobility in molten silicates is very low. In particular, previous studies have

pointed out that the diffusivity of Si^{4+} in glasses is lower when compared with other species like oxygen anions [29,35,41]. Even if in silicate minerals the diffusion coefficient of Mg^{2+} should be higher than oxygen ions [38], partial contribution of O^{2-} motion to conduction cannot be excluded. One could also speculate that material composition should remain constant by oxy-reductive reaction at the anodic and cathodic sites involving oxygen ions and molecular oxygen.

Figure 9 also shows a comparison between the resistivity measured during FS and an extrapolation of the resistivity behaviour observed before FS. It is possible to state that the resistivity during FS is much lower than that expected by previous measurements. This can be accounted for by the activation of different conduction mechanisms (i.e. diffusion paths with higher activation energy) during flash sintering, as a result of the increased sample temperature. Also a decrease in glass viscosity could be proposed as a possible explanation for this behaviour, in agreement with the electric field-induced softening observed by McLaren et al. [24].

In Figure 9 one can also observe that the estimated temperature reached by the samples is practically always lower than the lower liquidus temperature (1355 °C) of the ternary system $\text{Al}_2\text{O}_3 - \text{SiO}_2 - \text{MgO}$. Below this temperature it is impossible to obtain conventional efficient liquid phase sintering. In fact, the glassy phase would undergo a rather fast devitrification process, leading to the formation of a crystalline solid. In order to verify this statement, a GCA sample was sintered at 1350°C for 2 hours (heating rate =10°C/min); the sintering temperature was therefore very close to the liquidus temperature of the ternary system. A very porous microstructure was obtained as shown in Figure 12, having quite different features from those reported in Figures 4 and 5. In particular, a much higher amount of pores can be observed in the conventionally treated sample. This is also

confirmed by density measurements, which indicate a bulk density of 2.99 g/cm^3 and an amount of open porosity higher than 13% for the sample sintered without field. The formation of Mullite and of a magnesium-aluminum silicate (Sapphirine) from the glassy phase was determined by XRD analysis. Therefore, in the conventional sintering process, the glassy phase crystallizes; being the system at a temperature lower than the liquidus, this leads to the formation of a solid second phase. The absence of a stable liquid results in a non-efficient sintering process and densification is not particularly enhanced by the addition of glass. Also increasing the treating temperature up to 1370°C (soaking time = 2h, heating rate 10°C/min), the sintered body final density is only 3.11 g/cm^3 . In fact, at 1355°C a liquid phase is formed but, in such temperature range its content is very limited and does not allow a complete densification.

Therefore, by applying an external E-field it is possible to obtain an effective liquid phase sintering at temperatures that do not allow it by conventional methods, even after several hours. This suggests that the current flow or the rapid heating obtained by Joule effect during FS accelerates the densification phenomena more than the crystallization of the glass. In this way, an efficient and ultra-fast liquid phase sintering of the GCA material can be obtained at temperatures lower than the liquidus.

4 Conclusions

The main conclusions of the present work are:

- I. Flash Sintering can be successfully applied to materials characterized by the simultaneous presence of glassy and crystalline phase.
- II. The addition of magnesia silicate glass has a beneficial role on FAS behaviour of alumina. In particular, GCA sintered bodies are denser and characterized by lower

open porosity with respect to pure alumina. This also means that one can reduce the current density and power dissipation needed for densification.

- III. Power dissipation plots for magnesia silicate glass-containing alumina bodies show an unexpected change in the curvature, probably caused by partial crystallization of the glassy phase.
- IV. If a relative high voltage is applied (1500 V/cm), GCA samples are flash sintered at very low temperatures (650-750°C) compared with pure alumina (~920°C), although densification phenomena are not activated.
- V. The activation energy for conduction during FS is compatible with ionic diffusion in molten silicates. In particular, magnesium migration toward the cathode was observed.
- VI. Via E-Field application it is possible to obtain effective liquid phase sintering at sample temperatures lower than the liquidus of the corresponding ternary system.

References

- [1] J. A. Downs, V. M. Sglavo, Electric Field Assisted Sintering of Cubic Zirconia at 390°C, J. Am. Ceram. Soc. 96 (2013) 1342–1344.
- [2] M. Cologna, B. Rashkova, R. Raj, Flash Sintering of Nanograin Zirconia in <5 s at 850°C, J. Am. Ceram. Soc. 93 (2010) 3556–3559.
- [3] J. S.C. Francis, Rishi Raj, Flash-Sinterforging of Nanograin Zirconia: Field Assisted Sintering and Superplasticity, J. Am. Ceram. Soc. 95 (2012) 138–146.
- [4] R. I. Todd, E. Zapata-Solvas, R. S. Bonilla, T. Sneddon, P. R. Wilshaw, Electrical characteristics of flash sintering: thermal runaway of Joule heating, J. Eur. Ceram. Soc. 35 (2015) 1865–1877.

- [5] J. S. C. Francis, M. Cologna, R. Raj, Particle size effects in flash sintering, *J. Eur. Ceram. Soc.* 32 (2012) 3129–3136.
- [6] R. Muccillo, E.N.S. Muccillo, An experimental setup for shrinkage evaluation during electric field-assisted flash sintering: Application to yttria-stabilized zirconia, *J. Eur. Ceram. Soc.* 33 (2013) 515–520.
- [7] R. Muccillo, M. Kleitz, E. N.S. Muccillo, Flash grain welding in yttria stabilized zirconia, *J. Eur. Ceram. Soc.* 31 (2011) 1517–1521.
- [8] R. Baraki, S. Schwarz, O. Guillon, Effect of Electrical Field/Current on Sintering of Fully Stabilized Zirconia, *J. Am. Ceram. Soc.* 95 (2012) 75–78.
- [9] R. Raj, M. Cologna, J. S. C. Francis, Influence of Externally Imposed and Internally Generated Electrical Fields on Grain Growth, Diffusional Creep, Sintering and Related Phenomena in Ceramics, *J. Am. Ceram. Soc.* 94 (2011) 1941–1965.
- [10] S.K. Jha, R. Raj, The Effect of Electric Field on Sintering and Electrical Conductivity of Titania, *J. Am. Ceram. Soc.* 97 (2014) 527–534.
- [11] X. Hao, Y. Liu, Z. Wang, J. Qiao, K. Sun, A novel sintering method to obtain fully dense gadolinia doped ceria by applying a direct current, *J. Power Sources* 210 (2012) 86– 91.
- [12] M. Biesuz, G. Dell’Agli, L. Spiridigliozzi, C. Ferone, V.M. Sglavo, Conventional and field-assisted sintering of nanosized Gd-doped ceria synthesized by co-precipitation, *Ceram. Inter.* (2016) doi:10.1016/j.ceramint.2016.04.097.
- [13] R. Muccillo, E.N.S. Muccillo, M. Kleitz, Densification and enhancement of the grain boundary conductivity of gadolinium-doped barium cerate by ultra-fast flash grain welding, *J. Eur. Ceram. Soc.* 32 (2012) 2311–2316.
- [14] E. Zapata-Solvas, S. Bonilla, and P. R. Wilshaw, and R.I. Todd, Preliminary investigation of flash sintering of SiC, *J. Eur. Ceram. Soc.* 33 (2013) 2811–2816.

- [15] K. S. Naik, V. M. Sglavo, R. Raj, Flash sintering as a nucleation phenomenon and a model thereof, *J. Eur. Ceram. Soc.* 34 (2014) 4063–4067.
- [16] K.S. Naik, V.M. Sglavo, R. Raj, Field assisted sintering of ceramic constituted by alumina and yttria stabilized zirconia, *J. Eur. Ceram. Soc.* 34 (2014) 2435-2442.
- [17] E. Bichaud, J.M. Chai, C. Carry, M. Kleitz, M.C. Steil, Flash sintering incubation in $\text{Al}_2\text{O}_3/\text{TZP}$ composites, *J. Eur. Ceram. Soc.* 35 (2015) 2587–2592.
- [18] A. Gaur, V. M. Sglavo, Flash-sintering of MnCo_2O_4 and its relation to phase stability, *J. Eur. Ceram. Soc.* 34 (2014) 2391–2400.
- [19] A.L.G. Prette, M. Cologna, V. M., Sglavo, R. Raj 2011, Flash-sintering of Co_2MnO_4 spinel for solid oxide fuel cell applications, *J. Power Sources* 196 (2011) 2061-2065. [19] A. Gaur, V.M. Sglavo, Flash Sintering of $(\text{La}, \text{Sr})(\text{Co}, \text{Fe})\text{O}_3$ -Gd-Doped CeO_2 Composite", *J. Am. Ceram. Soc.*, 98 (2015) 1747–1752.
- [20] A. Gaur, V. M. Sglavo, 2014, Densification of $\text{La}_{0.6}\text{Sr}_{0.4}\text{Co}_{0.2}\text{Fe}_{0.8}\text{O}_3$ ceramic by flash sintering at temperature less than 100 °C, *J. Mater. Sci.* 49 (2014) 6321-6332.
- [21] M. Cologna, J. S. C. Francis, R. Raj, Field assisted and flash sintering of alumina and its relationship to conductivity and MgO-doping, *J. Eur. Ceram. Soc.* 31 (2011) 2827–2837.
- [22] M. Biesuz, V.M. Sglavo, Flash Sintering of Alumina: Effect of Different Operating Conditions on Densification, *J. Eur. Ceram. Soc.* 36 (2016) 2535-42.
- [23] Y. Zhang, J. Jung, J. Luo, Thermal runaway, flash sintering and asymmetrical microstructural development of ZnO and $\text{ZnO-Bi}_2\text{O}_3$ under direct currents, *Acta Mater.* 94 (2015) 87–100.
- [24] C. McLaren, W. Heffner, R. Tessarollo, R. Raj, and H. Jain, Electric field-induced softening of alkali silicate glasses, *Appl. Phys. Lett.* 107 (2015) 184101.

- [25] U. Scipioni Bertoli, Electrical Field Assisted viscous flow in soda alumina silicate glass, unpublished work, Master Thesis in Materials Engineering, University of Trento (2012).
- [26] M.N. Rahaman, Ceramic Processing and Sintering, Marcell Dekker, New York, USA.
- [27] J. Gonzalez-Julian, and O. Guillon, Effect of Electric Field/Current on Liquid Phase Sintering, *J. Am. Ceram. Soc.* 98 (2015) 2018–2027.
- [28] R. Freer, Diffusion in silicate minerals and glasses: a data digest and a guide to the literature, *Contr. Mineral. Petrol.* 76 (1981) 440-454.
- [29] D.J. Cherniak, Diffusion in quartz, melilite, silicate perovskite, and mullite, *Reviews Mineral. Geochem.* 72 (2010) 735-756.
- [30] T. Dunn, Cation diffusion in Olivine. Cobalt and Magnesium, M. Morioka, *Geochimica et Cosmochimica Acta* 46 (1982) 2293-99.
- [31] H. Bracht, E.E. Haller and R. Clark-Phelps, Silicon self-diffusion in isotope heterostructures, *Physical Review Letters* 81 (1998) 393-396.
- [32] C. Barry Carter, M. Grant Norton, *Ceramic Materials: Science and Engineering*, Springer, 2007, pp. 532-533.
- [33] R. H. Doremus, *Glass Science*, Wiley, New York, USA, 1994.
- [34] R. J. Maurer, Deviations from Ohm's Law in Soda Lime Glass, *J. Chem. Phys.* 9 (1941) 579-584.
- [35] Y. Oishi, R. Terai and H. Ueda, Oxygen diffusion in liquid silicates and relation to their viscosity, in *Material Science Research, Volume 9 Mass Transport Phenomena in Ceramics*, Plenum Press, New York, USA, 1975.
- [36] Y. Zhang, H. Ni and Y. Chen, Diffusion in silicate melts, *Reviews Mineral. Geochem.* 72 (2010) 311-408.
- [37] E.L. Williams, Diffusion of oxygen in fused silica, *J. Am. Ceram. Soc.* 48 (1965) 190-194.

- [38] Y. Zhang and H. Ni, Diffusion of H, C and O components in silicate melts, *Reviews Mineral. Geochem.* 72 (2010) 171-255.
- [39] T. Dunn, Oxygen diffusion in three silicate melts along the join diopside - anorthite, *Geochimica et Cosmochimica Acta* 46 (1982) 2293-99.
- [40] C.E. Lesher, R.L. Hervig, D. Tinker, Self diffusion of network formers (silicon and oxygen) in naturally occurring basaltic liquid, *Geochimica et Cosmochimica Acta* 60 (1996) 405-413.
- [41] H. A. Shaeffer, Transport phenomena and diffusion anomalies in glass, *Ceramic Materials* 64 (2012) 156-161.
- [42] K. Sunder, M. Grofmeier, R. Staskunaite, H. Bracht, Dynamics of Network Formers and Modifiers in Mixed Cation Silicate Glasses, *J. Phys. Chem.* 224 (2010) 1677–1705.
- [43]
<http://www.engineering.com/Library/ArticlesPage/tabid/85/ArticleID/151/Emissivity.aspx>
- [44] E.C. Guyer, *Handbook of applied thermal design*, Hamilton Printing, Castleton, NY, USA, 1999, pp. 1-89.
- [45] F. Kreith, *The CRC handbook of thermal engineering*, CRC Press LLC, Danvers, USA, 2000, pp. 3-71.

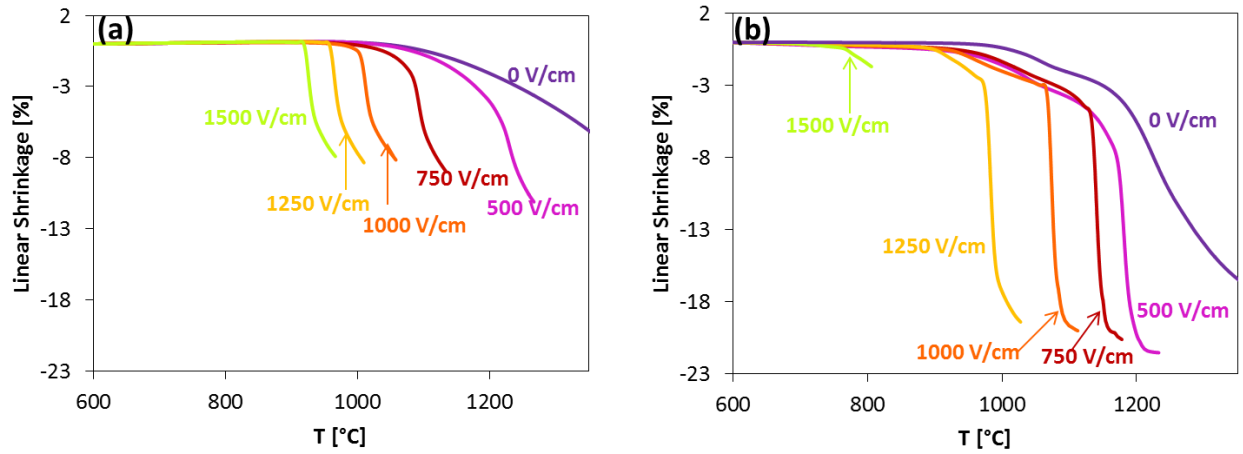


Figure 1: Dilatometric plot for pure alumina (a) and glass-containing alumina (b) samples sintered under different electric fields and current limit of 2mA/mm^2 .

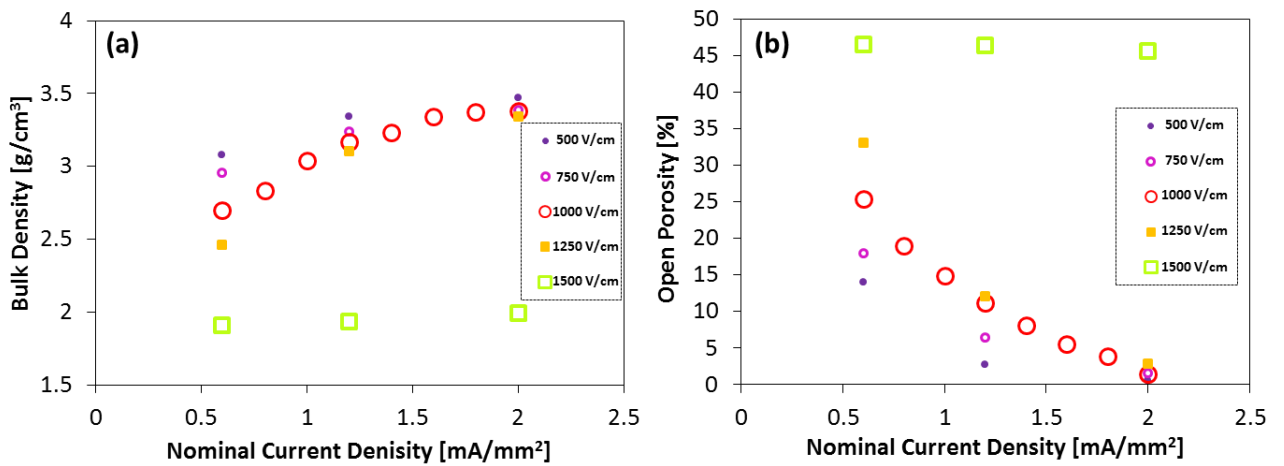


Figure 2: Bulk density (a) and open porosity (b) for GCA sintered bodies as a function of current density.

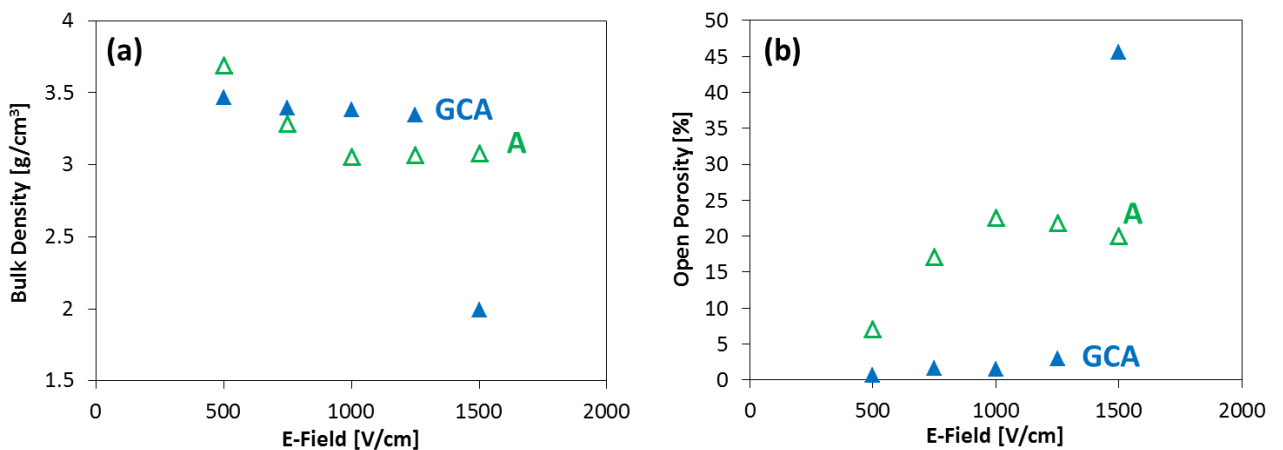


Figure 3: Bulk density (a) and open porosity (b) for glass-containing alumina (GCA) and pure alumina (A) sintered bodies as a function of current density.

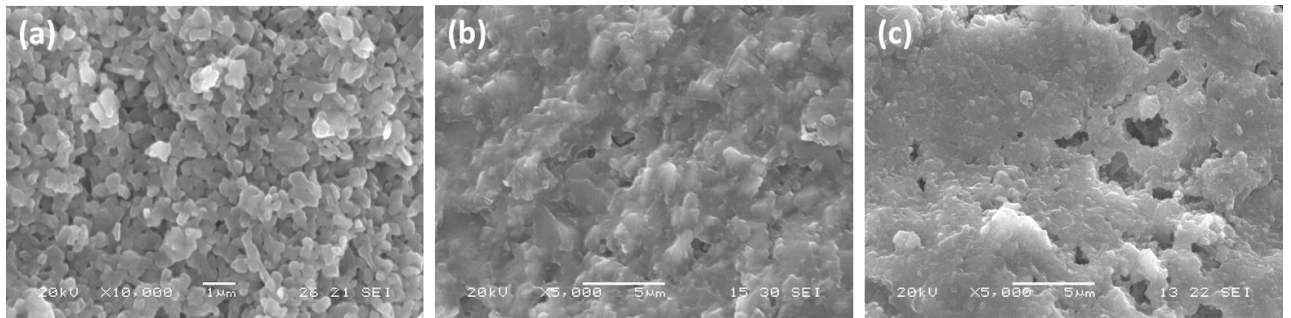


Figure 4: SEM micrographs of the fracture surface of pure alumina (a), glass-containing alumina sample treated under 1000 V/cm and 2 mA/mm² (b) and glass-containing alumina sample flash sintered under 1000 V/cm with lower current density (0.6 mA/mm²) (c).

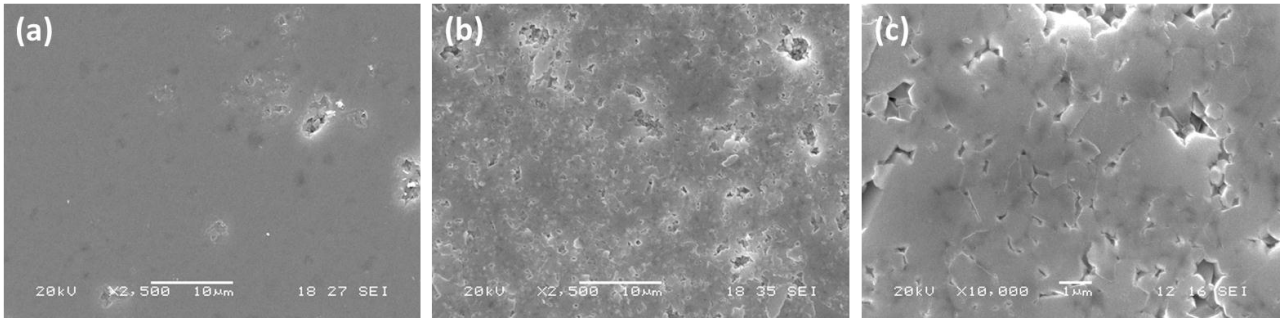


Figure 5: SEM micrographs of polished (a) and polished and HF etched (b,c) surface (at different magnification) for glass-containing alumina samples treated using 1000 V/cm and 2 mA/mm².

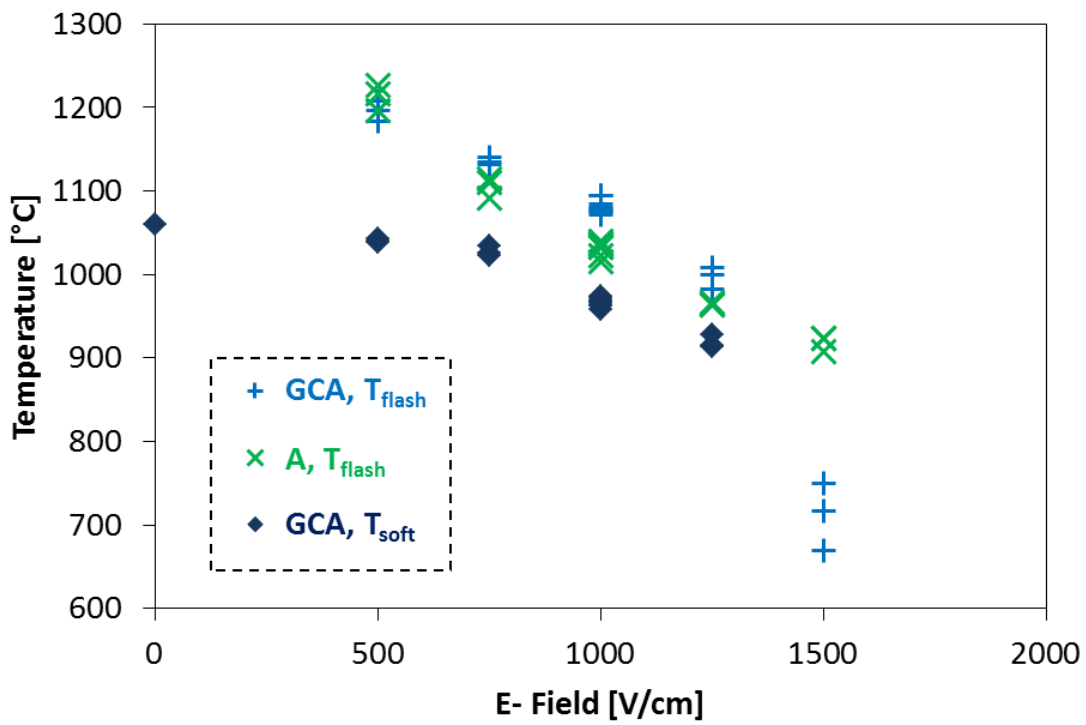


Figure 6: Onset temperature for flash sintering for pure alumina and GCA. The temperature at which the maximum shrinkage rate is reached during glass softening is also shown.

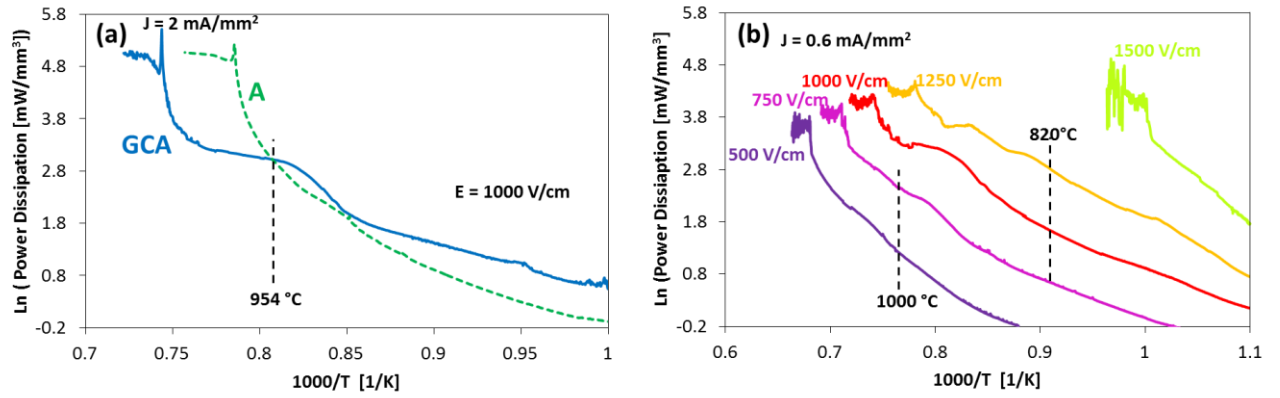


Figure 7: Specific power dissipation as a function of the furnace temperature: (a) comparison between pure alumina and glass-containing material flash sintered under 1000 V/cm and 2 mA/mm²; (b) power dissipation during flash sintering of GCA samples treated under different fields using a current limit of 0.6 mA/mm².

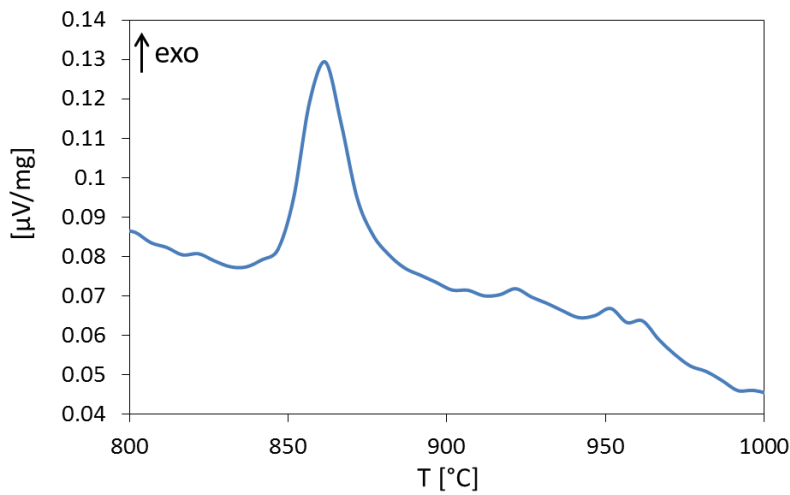


Figure 8: DSC analysis of the GCA powder (heating rate = 20°C/min).

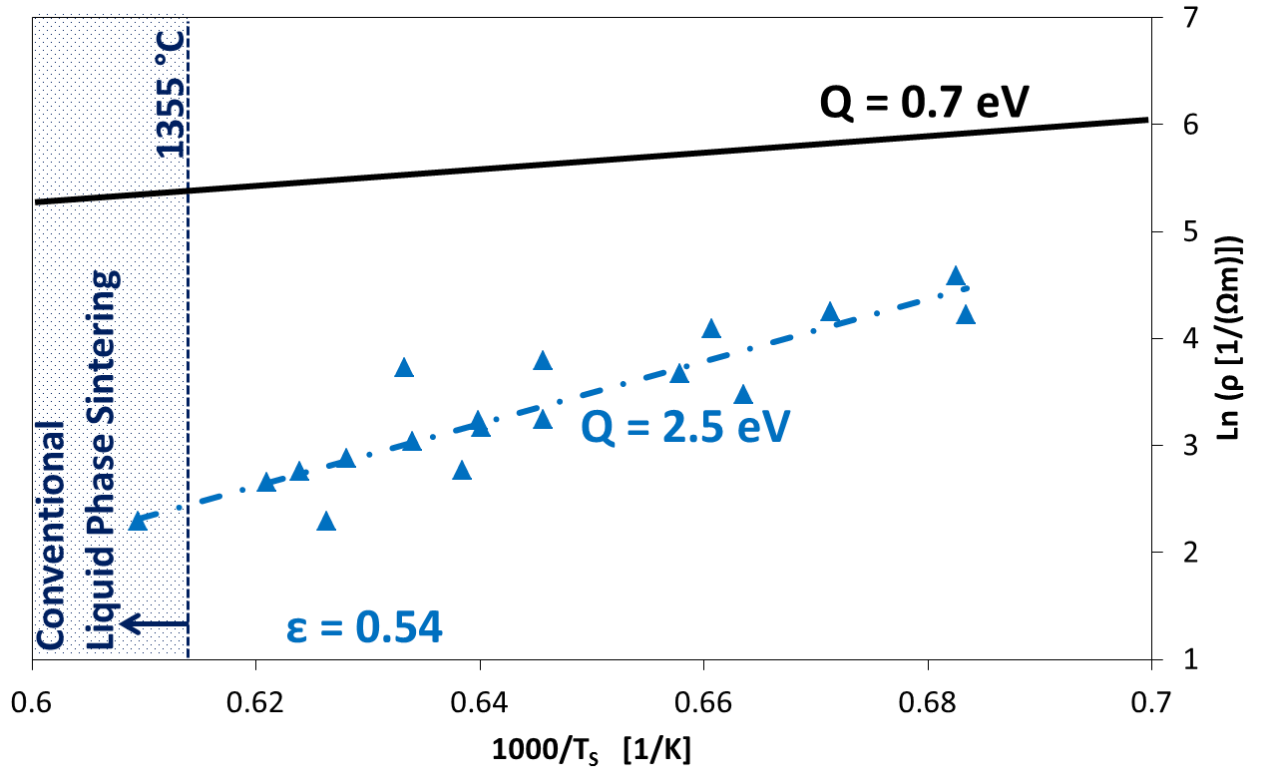


Figure 9: Resistivity as a function of sample temperature during flash sintering, assuming an emissivity of 0.54. The black continuous line represents the extrapolation at high temperature of the resistivity measured before flash sintering, using the data collected at 500 - 1250 V/cm ($Q = 0.7$ eV). The dashes-dot line is the fitting curve, obtained with an activation energy of 2.5 eV. All but one of the points correspond to sample temperatures lower than the liquidus of the ternary system (1355°C).

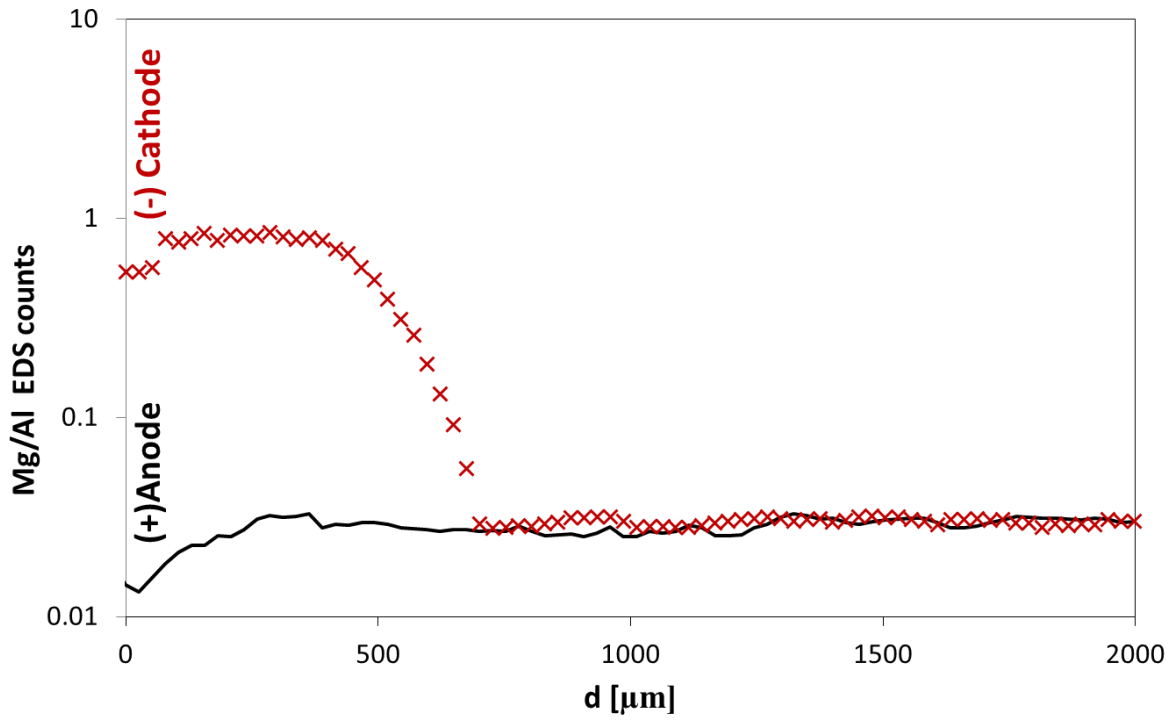


Figure 10: Ratio between magnesium and aluminum EDS counts at different distances from anode (crosses) and cathode (continuous line) in the sample treated with 750 V/cm and 2 mA/mm².

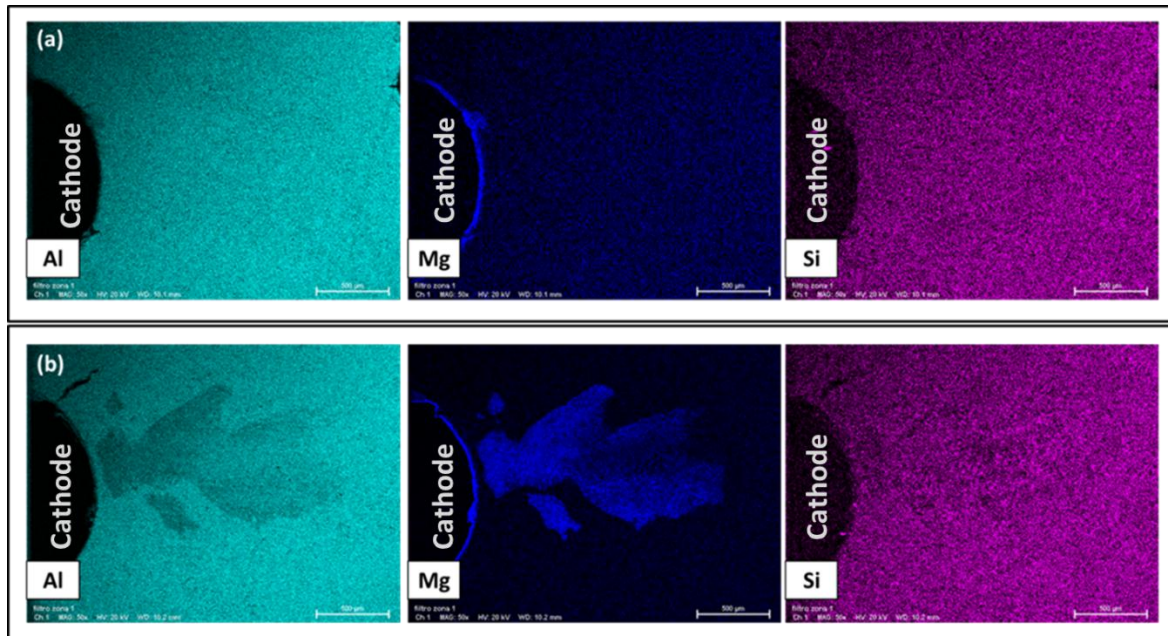


Figure 11: EDS concentration map for Al, Mg and Si close to the cathode of sample treated with 2 mA/mm² under 500 (a) and 1000 V/cm (b).

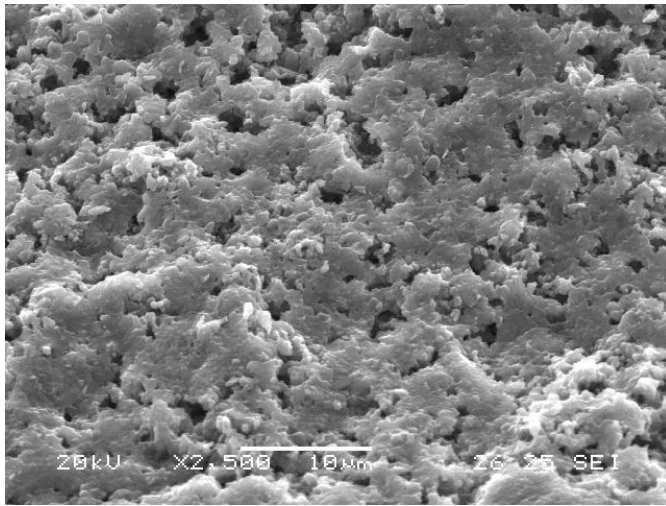


Figure 12: SEM micrograph of a conventionally sintered glass-containing sample ($T = 1350^{\circ}\text{C}$, $t = 2\text{ h}$).